Interacting dark states with enhanced nonlinearity in an ideal four-level tripod atomic system

Yanxu Han,[1] Jintao Xiao,[1] Yonghong Liu,[1] Chunhong Zhang,[1] Hai Wang,[1,*] Min Xiao,[1,2] and Kunchi Peng[1]
[1]*The State Key Laboratory of Quantum Optics and Quantum Optics Devices, Institute of Opto-Electronics, Shanxi University, Taiyuan, 030006, People's Republic of China*
[2]*Department of Physics, University of Arkansas, Fayetteville, Arkansas 72701, USA*
(Received 21 October 2007; published 21 February 2008)

We present an experimental system to generate large cross-phase modulation (XPM) in cold rubidium atoms. By using an efficient state-preparation technique in the ^{87}Rb $D1$ line, an ideal four-level tripod-type atomic system is formed, which generates large cross-Kerr nonlinearity via interacting dark states in this system. The induced phase shift due to XPM for the probe beam is measured for different trigger beam intensities, which is the key to achieving conditional quantum phase gates and many other applications in quantum information processing.

DOI: 10.1103/PhysRevA.77.023824 PACS number(s): 42.50.Gy, 42.65.−k, 32.80.−t

As the electromagnetically induced transparency (EIT) [1–3] or dark state [4] is the property of three-level atomic systems interacting with two laser fields, properly arranged four-level atomic systems (such as N- [5], inverted-Y- [6], tripod-type [7], and double-Λ [8] systems) together with three or more laser beams can generate two EIT windows or create double dark states. Double dark states in a four-level atomic system (with a three-level Λ-type system dressed by a RF field in the ground state for the coupling beam) have been theoretically predicted [9] and an efficient nonlinear sideband generation in such a four-level system has also been experimentally demonstrated [10]. Such double dark states can interact and produce large cross-phase modulation (XPM) between the laser beams [5–7], which is essential to construct quantum phase gates [6,7,11–13] for quantum computing and quantum information processing. Recently, several interesting applications of XPM nonlinearities, such as generating cluster states [14], GHZ states [15], and nondestruction Bell-state detecting [16] via quantum nondemolition measurement, have been proposed in literature.

Although conditional phase shift has been experimentally demonstrated in a cavity-QED system more than ten years ago [11] and many schemes were proposed to construct quantum phase gates in multilevel atomic systems [6,7,12,13], a true experimental demonstration of such conditioned quantum phase gates still eludes researchers in the laboratories. Large cross-Kerr nonlinearities have been predicted in various four-level atomic systems [5–7,12,13] but experimental complications, such as complicated multi-Zeeman sublevels, Doppler effect in hot atoms, difficult in preparing needed initial atomic state populations, and relatively low atomic density in cold atomic samples, have made it very difficult to realize the proposed ideal systems in real atoms. More recently, a new configuration with combined N-type and tripod-type subsystems was proposed to generate large XPM with matched slow propagating weak pulses [17]. This five-level atomic system is simplified from the realistic $D1$ line of ^{87}Rb by using a large magnetic field, which is quite complicated and hard to realize for cold atoms in a standard magneto-optical trap (MOT).

In this work, we propose and experimentally demonstrate an ideal four-level tripod-type atomic system with a well-prepared initial atomic state in the $D1$ line of ^{87}Rb in a cold MOT without employing high magnetic field. This closed four-level tripod-type atomic system, as shown in Fig. 1(a), can generate large XPM between the trigger beam Ω_T (right circularly polarized, connecting states $5S_{1/2}$, $F=2$ to $5P_{1/2}$, $F'=1$) and the probe beam Ω_P (left circularly polarized, connecting states $5S_{1/2}$, $F=1$ to $5P_{1/2}$, $F'=1$). By employing the state preparation technique demonstrated previously [18] with the coupling (left circularly polarized, connecting states $5S_{1/2}$, $F=2$ to $5P_{1/2}$, $F'=1$), trigger, and a right circularly polarized pumping (connecting states $5S_{1/2}$, $F=1$ to state $5P_{3/2}$, $F'=1$) beams, most of the atoms (>95%) in Zeeman sublevels $m=-1,0,+1$ of the $5S_{1/2}$, $F=1$ level are prepared in the ground state $|0\rangle$ $(m=+1)$.

Energy levels $|0\rangle$-$|1\rangle$-$|2\rangle$-$|3\rangle$ form an isolated four-level tripod system. Since the atoms are initially prepared in the $|0\rangle$ state, as checked by the state-preparation procedure [18], this four-level tripod system is the only relevant one needed to be considered here. When $\Omega_T/\Omega_C \ll 1$ (and $\Omega_P \ll \Omega_T \ll \Omega_C$), most of the atomic populations on the ground states ($5S_{1/2}$, $F=2$ and $F=1$) will be pumped to the states $|1\rangle$ and $|0\rangle$ $(\rho_{11} \approx \rho_{00})$ [7], and some of them will be trapped in the state

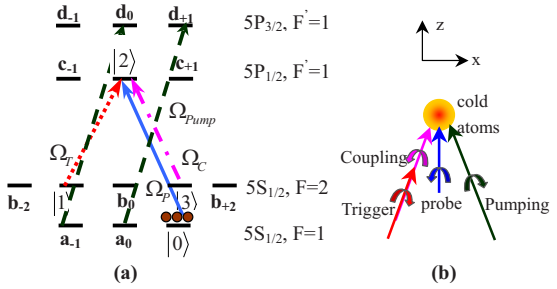

FIG. 1. (Color online) (a) Relevant energy diagram of the $D1$ line in the ^{87}Rb atom. Solid line: transition for the left circularly polarized probe laser beam (Ω_P); dotted line: transition for the right circularly polarized trigger beam (Ω_T); dashed-dot line: transition for the left circularly polarized coupling beam (Ω_C); dashed line: transition for the right circularly polarized pumping beam (Ω_{pump}). (b) Experimental arrangement of laser beams.

*Corresponding author. wanghai@sxu.edu.cn

$|b_{-2}\rangle$, which will not interact with light. This is a typical tripod system with one strong coupling beam (Ω_C) and two weak probe beams (Ω_P and Ω_T), which can be considered as two three-level Λ-type EIT systems sharing the same coupling beam and has been proposed for constructing the conditional polarization phase gates [7]. When $\Omega_T/\Omega_C \rightarrow 1$, most of the atomic populations in the chosen tripod four-level system are prepared to the state $|0\rangle$ [19]. In such a case, two separate EIT windows (when the frequency detunings are different) will be generated or two dark states formed, which interact strongly when both of them are on resonance. We will vary Ω_T in the experiment to study the evolution of cross-Kerr nonlinearity between these two interesting limits. The atomic system for the four relevant energy levels interacting with the appropriate laser beams can be described by the system Hamiltonian [7]

$$H = \hbar\Delta_P|2\rangle\langle 2| + \hbar(\Delta_P - \Delta_T)|1\rangle\langle 1| + \hbar(\Delta_P - \Delta_C)|3\rangle\langle 3| - \frac{\hbar}{2}[\Omega_P|2\rangle\langle 0| + \Omega_T|2\rangle\langle 1| + \Omega_C|2\rangle\langle 3| + cc] \quad (1)$$

where $\Delta_P = \omega_P - \omega_{20}$, $\Delta_C = \omega_C - \omega_{23}$, and $\Delta_T = \omega_T - \omega_{21}$ are the frequency detunings of the probe beam, coupling beam, and trigger beam, respectively. The susceptibility of the probe beam can be written as

$$\chi_p = -P_0 N_{F1}\rho_{02}|\mu_{02}|^2/(\hbar\varepsilon_0\Omega_p), \quad (2)$$

where $P_0 N_{F1}$ is the percentage of population on state $|0\rangle$ and μ_{02} is the dipole moment between states $|0\rangle$ and $|2\rangle$. This expression includes all the linear and nonlinear contributions due to the coupling and trigger beams. Here, we are only interested in the XPM defined as

$$\chi_p = \chi_p^{(1)} + \chi_p^{(3)}|E_T|^2 + \cdots, \quad (3)$$

which gives the leading cross-Kerr nonlinear term due to the trigger beam. Full simulation of the system (with all the energy levels as shown in Fig. 1(a) can give all the linear and nonlinear susceptibilities of the system and steady-state populations in each state, which confirms the simplified four-level tripod-type system used here and is used to compare with our experimentally measured results. When the frequency detunings of the coupling and trigger beams are different $\Delta_T \neq \Delta_C$, and $\Omega_C \approx \Omega_T$, there are two distinct EIT windows for the probe beam. As the two EIT windows are tuned to overlap in frequency (by tuning one of the frequency detunings), the two dark states will interact and generate enhanced cross-Kerr nonlinearity. As the intensity of the trigger beam is adjusted, the XPM phase shift experienced by the probe beam will increase, the slope of which gives the cross-Kerr nonlinear coefficient. Such large XPM phase shift is the necessary mechanism to achieve quantum phase gates and for many other applications.

The experiment is carried out in cold ^{87}Rb atoms trapped in a standard MOT, which is the same as in Ref. [20]. The trigger and coupling laser beams are from one external-cavity diode laser, and the probe beam is from another external-cavity diode laser. As shown in Fig. 1(b), a weak left circularly polarized probe beam propagates along the z axis through the cold atoms, while a strong left circularly polarized coupling beam and a right circularly polarized trigger beam propagate along one direction with a positive small angle (about 2°) relative to the probe beam through the cold atoms. The diameters of the coupling, trigger, and probe beams are about 1.4, 2, and 0.5 mm, respectively, at the position of cold atoms. To prepare atoms into the desired Zeeman sublevel, we let the right circularly polarized pumping beam propagates through the cold atoms with a negative small angle (about 2°) relative to the probe beam. The power of the pumping beam is set at about 4 mW with a diameter of ~2 mm (which overlaps with the coupling and probe beams at the cold atomic cloud). A uniform, weak magnetic field of about 150 mG in the z direction is applied at the location of the cold atoms. During the experiment, the on-off sequence of the trapping, repumping, coupling, trigger, and pumping beams are controlled by five acousto-optical modulators. The coupling, trigger, and pumping beams are switched on at the same time as the MOT is turned off. The probe beam is always on in the experimental procedure since it is very weak (about 3.6 μW) and will not disturb the atomic trapping and cooling process. We scan the probe frequency and measure the probe light signal after it passes through the cold atoms at the same time as the MOT is turned off, ~140 μs later.

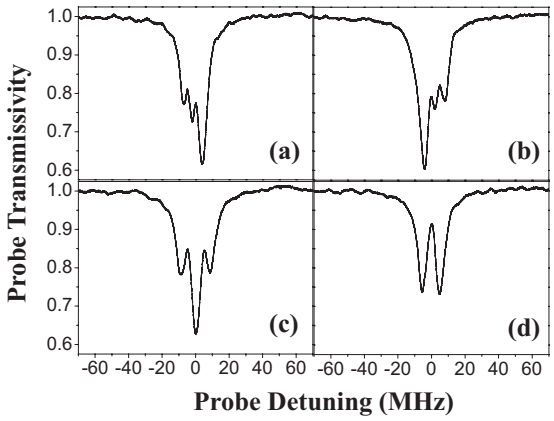

FIG. 2. Measured probe transmissivity as a function of the probe frequency detuning. The frequency detunings are (a) Δ_C=5 MHz, Δ_T=0 MHz; (b) Δ_C=0 MHz, Δ_T=−5 MHz; (c) Δ_C=5 MHz, Δ_T=−5 MHz; (d) Δ_C=Δ_T=0 MHz. The Rabi frequencies of coupling and trigger beams are $\Omega_T \approx \Omega_C \approx 7$ MHz.

Figure 2 shows the dual EIT windows in the system for different coupling and trigger beam frequency detunings. When the frequency detunings Δ_C and Δ_T are different, the two EIT windows are separate in frequency [Figs. 2(a)–2(c)]. The overlapping EIT windows shown in Fig. 2(d) correspond to interacting dark states in the system, which greatly enhance EIT, as well as XPM nonlinearity. As easily seen in Figs. 2(a)–2(c), interference between the two EIT windows (or dark states) can actually generate increased absorption at certain frequencies [such as at Δ_P=0 in Fig. 2(c)]. The change of absorption at Δ_P=0 between Figs. 2(c) and 2(d) can be used to obtain an all-optical switching.

Figure 3(a) presents the EIT signal when Ω_T is blocked, which is a simple three-level Λ-type EIT system ($|0\rangle$-$|2\rangle$-$|3\rangle$) with a coupling beam Rabi frequency of Ω_C=6.5 MHz. The

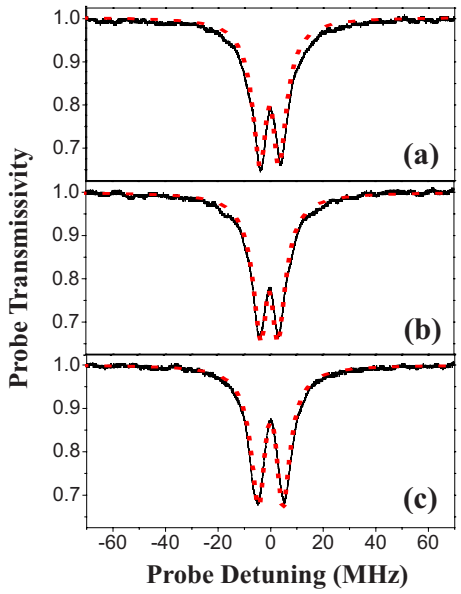

FIG. 3. (Color online) The probe transmission for (a) only with coupling beam, (b) only with trigger beam, and (c) with both coupling and trigger beams, respectively. The (red) dotted lines are the theoretically calculated results with the parameters Ω_C=6.5 MHz, Ω_T=5.7 MHz, and $P_0N_{F1}=0.28\times10^{11}/\mathrm{cm}^3$ for (a) and (b), $P_0N_{F1}=0.20\times10^{11}/\mathrm{cm}^3$ for (c). Other parameters are γ_{ab}=1.8 MHz and γ_{ac}=3.6 MHz (γ_{ab} and γ_{ac} include the laser linewidths).

EIT signal is intentionally kept small (by using a lower coupling beam intensity) to demonstrate the EIT enhancement. Similarly, when Ω_C is blocked, an EIT signal is seen in Fig. 3(b) from another three-level Λ-type system ($|0\rangle$-$|2\rangle$-$|1\rangle$) with trigger beam Rabi frequency of Ω_T=5.7 MHz is seen in Fig. 3(b). When both Ω_C and Ω_T are on with the same intensities as before [Figs. 3(a) and 3(b)], the total EIT signal [as shown in Fig. 3(c)] becomes much larger than each individual one. The individual EIT signals [Figs. 3(a) and 3(b)] were chosen to maximize the change of the EIT signal when both beams (Ω_T and Ω_C) are on. Theoretically calculated results (dotted lines) match well with the experimental data (solid lines). It is noted that the atomic population $(0.28\times10^{11}/\mathrm{cm}^3)$ in $|0\rangle$ state with only one (trigger or coupling) beam on is larger than that $(0.20\times10^{11}/\mathrm{cm}^3)$ with both (coupling and trigger) beams on. The reason is that the chosen four-level tripod system is an open system in the Rb $D1$ line, and the atomic populations in this system will become smaller due to stronger optical pumping with the coupling and trigger beams simultaneously turned on.

More importantly, not only the linear EIT effect can be increased due to the interacting dark states, the cross-Kerr nonlinearity can also be greatly modified and enhanced under appropriate conditions. The dispersion curves of the probe beam for the EIT and the tripod systems can be measured by using a Mach-Zehnder interferometer, as shown in Fig. 4. The Mach-Zehnder interferometer is formed by using two beam displacing polarizers, BD1 and BD2. The linearly polarized input probe beam (with a chosen polarization angle) is separated into two beams by BD1. One of them is p polarized and another is s polarized. After going through the

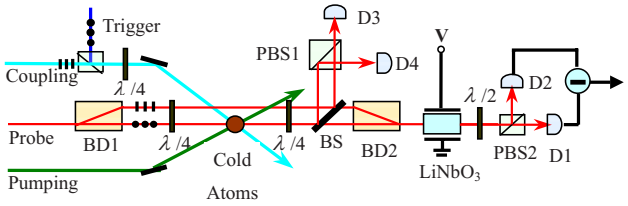

FIG. 4. (Color online) Mach-Zehnder interferometer to detect the dispersion of the probe beam in the system.

BD1, the s- and p-polarized probe beams propagate in parallel. The s-polarized probe beam is weak (~3.6 μW) to be used as the probe beam and the p-polarized beam is stronger (~82.6 μW) to be used as the reference beam in the Mach-Zehnder (MZ) interferometer. The s- and p-polarized probe beams become left and right circularly polarized, respectively, after going through a $\lambda/4$ wave plate. Only the originally s-polarized probe beam transmits through the cold atoms, which is changed back into an s-polarized beam by another $\lambda/4$ wave plate after going through the cold atomic sample. The original p-polarized probe beam does not transmit through the cold atoms, and is changed back to the p polarization by the $\lambda/4$ wave plate behind the cold atoms. A beam splitter (BS) is used to reflect part of the weak and strong probe beams into PBS1, and then detected by $D3$ and $D4$ detectors, respectively, which give the signal intensities of the weak and strong probe beams. The transmitted weak (s-polarized) and strong (p-polarized) beams overlap at the end of BD2 and then combine into one beam again. The p- and s-polarized components in the combined beam will both be rotated 45° by a $\lambda/2$ wave plate. This combined beam is then split into two beams with the same power by PBS2. So, the two beams detected by $D1$ and $D2$ include both the weak probe beam (going through atoms) and the strong (reference) beam, as in a standard MZ interferometer. The detectors $D1$ and $D2$ form a homodyne arrangement, whose differential signal ΔI_d is given by [3]

$$\Delta I_d \propto 2|E_R||E_P|e^{-\alpha(\omega)l/2}\cos[\phi_R + k_p n_p(\omega)l], \qquad (4)$$

where k_p is the probe wave vector, l is the medium length, and n_p is the index of refraction for the probe beam. E_P is the probe field, which will acquire a phase shift $k_p n_p l$ when it passes through the cold atoms. $\alpha(\omega)$ is the absorption coefficient for the probe field. E_R is the strong (reference) field. ϕ_R is the reference phase of the MZ interferometer, which is reset to $\pi/2$ by a $LiNbO_3$ crystal. When the probe frequency scans across the EIT resonance, we can record the data detected by $D1$, $D2$, $D3$, and $D4$ and then calculate the probe phase shift as a function of its frequency detuning according to Eq. (4).

The measured dispersion curves for without and with the trigger beam are plotted in Figs. 5(a) and 5(b), respectively, with the parameters the same as used in Fig. 3. The results show a significant enhancement in dispersion when trigger beam is applied, and theoretically calculated results (dotted lines) match well with the experimental data (solid lines). This dispersion change is directly linked to the XPM nonlin-

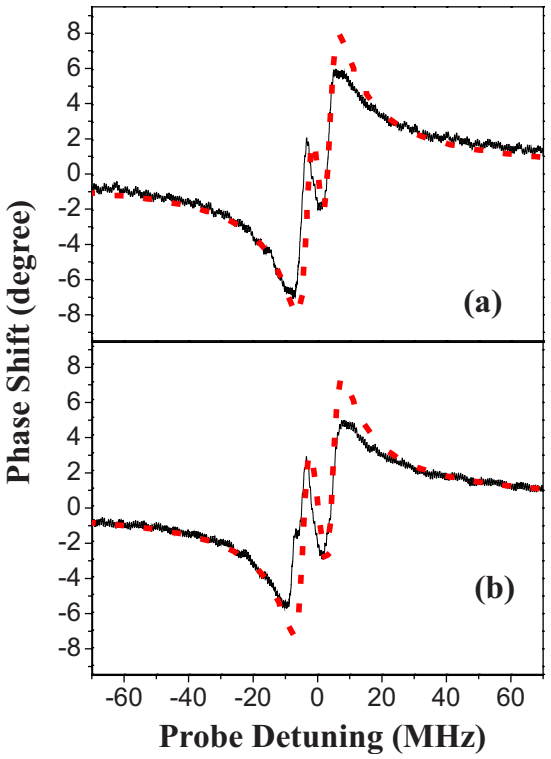

FIG. 5. (Color online) Measured dispersion curves (solid line) for without (a) and with (b) the trigger beam, (red) dotted lines are the theoretically calculated results with the parameters Ω_C =6.5 MHz and Ω_T=5.7 MHz. Other parameters are the same as in Fig. 3.

earity [17] and can be converted into cross-Kerr nonlinear phase shift Φ_p^N as

$$\Phi_p^N = k_p l(\, n_p|_{(I_T\neq 0)} - \, n_p|_{(I_T=0)}) = k_p l \Delta n_p = k_p l I_T n_{2p}, \quad (5)$$

where Δn_p is the difference between the index of refractions for the probe beam when the trigger beam is switched on and off. I_T is the intensity of the trigger beam, and n_{2p} is the Kerr nonlinear index of refraction. This nonlinear phase shift Φ_p^N can be controlled by the intensity of the trigger beam, which is experimentally measured and presented in Fig. 6. As one can see, there is a maximal value of Δn_p for certain trigger beam intensity. The slope of n_p vs I_T curve gives the effective n_{2p} value, which is 7.2×10^{-5} cm^2/W under the current experimental conditions. For a given trigger beam intensity of 8.8 mW/cm^2, the XPM phase shift Φ_p^N can reach 1×10^{-2} rad, which satisfies the requirement for generating the GHZ states [15]. Of course, the XPM phase shift can be increased by using a high intensity or tightly focused trigger beam.

The factors limiting the XPM phase shift in the current experimental setup include relatively low density of trapped cold atoms, relatively broad laser linewidths (~2 MHz for coupling laser and ~1.5 MHz for probe laser), and residual atomic populations trapped in the states other than the closed four-level tripod system due to CPT in the $5S_{1/2}$, F=2 states. One can improve these technical problems by optimizing the current MOT to reach a higher atomic density (from current

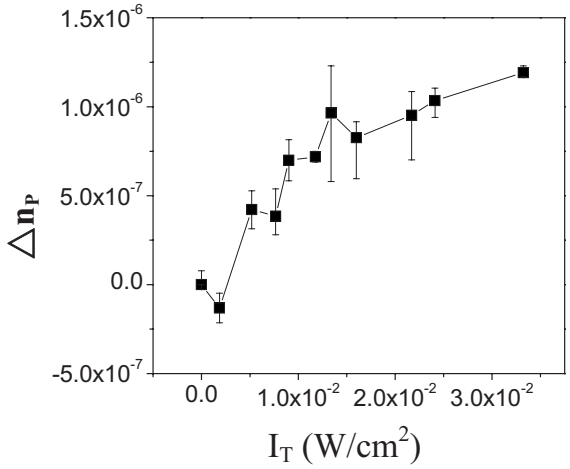

FIG. 6. Measured phase shifts as a function of the trigger beam intensity.

10^{10}/cm^3 to 10^{11}/cm^3). The laser linewidths can be suppressed down to 50 kHz by feedback locking and phase locking the diode lasers used in the experiment.

Although the current experimentally measured XPM phase shift is still not large enough to achieve true conditional quantum phase gates, it is, however, a large step towards such a goal, since it presents an isolated four-level tripod system with well-prepared (and desired) initial atomic states needed to build the ultimate quantum phase gates. Also, by adjusting the ratio of Ω_T/Ω_C the current system can be changed from a tripod system with two weak probe fields and one strong coupling beam into a tripod system with two strong coupling beams and one weak probe beam, which can serve for different applications.

The current tripod system of enhancing cross-XPM nonlinearity has a very important advantage over the one using the N-type system [21], i.e., having large XPM without accompanying absorption. Also, there are EIT windows simultaneously for both the probe and trigger fields, which make the group velocities of these fields to match, and such lead to a longer interaction time to acquire a large cross-phase shift [7]. Actually, due to the increased EIT with increasing Ω_T, the absorption is greatly reduced, which will greatly improve the figure of merit of the system defined by $\Phi_{NL}/\alpha l$ [22] for realizing the conditioned quantum phase gates.

In summary, we have experimentally demonstrated interacting dark states in an isolated four-level tripod system with a well-prepared initial atomic state in the cold ^{87}Rb $D1$ line. To the best of our knowledge, this is the first experimental demonstration of a true four-level tripod system with a well-prepared atomic state in the multi-Zeeman sublevel systems. Enhanced EIT and XPM nonlinearity were both experimentally measured in such a state-prepared atomic system. Effective Kerr-cross nonlinear index was determined from the measured slope of nonlinear index as a function of trigger beam intensity. The experimentally measured results compare well with calculations from the simplified four-level atomic system with realistic parameters. Such enhanced XPM nonlinearity can have important applications in building quantum phase gates [6,7,11–13], realizing quantum measurements [16], and generating cluster states [14] and

GHZ states [15] for quantum information processing. Also, the double dark states in four-level atomic systems can be used to create dual EIT windows for simultaneously generating efficient four-wave and six-wave mixing processes [23].

We acknowledge funding supports by the National Natural Science Foundation of China (Grants No. 60325414, No. 60578059, and No. 10640420195), 973 Program (Grant No. 2006CB921103), and NSF of Shanxi Province (Grant No. 2007011004).

[1] S. E. Harris, Phys. Today **50**, 36 (1997).
[2] J. Gea-Banacloche, Y. Q. Li, S. Z. Jin, and M. Xiao, Phys. Rev. A **51**, 576 (1995).
[3] M. Xiao, Y. Q. Li, S. Z. Jin, and J. Gea-Banacloche, Phys. Rev. Lett. **74**, 666 (1995).
[4] M. Fleischhauer and M. D. Lukin, Phys. Rev. Lett. **84**, 5094 (2000).
[5] H. Schmidt and A. Imamoglu, Opt. Lett. **21**, 1936 (1996).
[6] A. Joshi and M. Xiao, Phys. Rev. A **72**, 062319 (2005).
[7] S. Rebic, D. Vitali, C. Ottaviani, P. Tombesi, M. Artoni, F. Cataliotti, and R. Corbalan, Phys. Rev. A **70**, 032317 (2004).
[8] G. Wasik, W. Gawlik, J. Zachorowski, and Z. Kowal, Phys. Rev. A **64**, 051802(R) (2001).
[9] M. D. Lukin, S. F. Yelin, M. Fleischhauer, and M. O. Scully, Phys. Rev. A **60**, 3225 (1999).
[10] S. F. Yelin, V. A. Sautenkov, M. M. Kash, G. R. Welch, and M. D. Lukin, Phys. Rev. A **68**, 063801 (2003).
[11] Q. A. Turchette, C. J. Hood, W. Lange, H. Mabuchi, and H. J. Kimble, Phys. Rev. Lett. **75**, 4710 (1995).
[12] C. Ottaviani, D. Vitali, M. Artoni, F. Cataliotti, and P. Tombesi, Phys. Rev. Lett. **90**, 197902 (2003).
[13] D. Petrosyan and Yu. P. Malakyan, Phys. Rev. A **70**, 023822 (2004).
[14] S. G. R. Louis, K. Nemoto, W. J. Munro, and T. P. Spiller, New J. Phys. **9**, 193 (2007).
[15] G.-S. Jin, Y. Lin, and B. Wu, Phys. Rev. A **75**, 054302 (2007).
[16] S. D. Barrett, P. Kok, K. Nemoto, R. G. Beausoleil, W. J. Munro, and T. P. Spiller, Phys. Rev. A **71**, 060302(R) (2005).
[17] Z. B. Wang, K. P. Marzlin, and B. C. Sanders, Phys. Rev. Lett. **97**, 063901 (2006).
[18] B. Wang, Y.-X. Han, J.-T. Xiao, X.-D Yang, C.-H. Zhang, H. Wang, M. Xiao, and K.-C. Peng, Phys. Rev. A **75**, 051801(R) (2007).
[19] E. Paspalakis and P. L. Knight, J. Opt. B: Quantum Semiclassical Opt. **4**, S372 (2002).
[20] B. Wang, Y.-X. Han, H. Wang, and M. Xiao, Opt. Lett. **31**, 3647 (2006).
[21] H. Kang and Y. Zhu, Phys. Rev. Lett. **91**, 093601 (2003).
[22] Y.-F. Chen, C.-Y. Wang, S.-H. Wang, and Ite A. Yu, Phys. Rev. Lett. **96**, 043603 (2006).
[23] Y. P. Zhang, A. W. Brown, and Min Xiao, Phys. Rev. Lett. **99**, 123603 (2007).